Chapter 15

Metal–Semiconductor Hybrid Nano-Heterostructures for Photocatalysis Application

Nimai Mishra

Additional information is available at the end of the chapter

http://dx.doi.org/10.5772/62636

Abstract

This chapter will address the development of colloidal synthesis of hybrid metal–semiconductor nanocrystals and their application in the field of photocatalysis. Despite the plethora of examples of different-shaped metal–semiconductor nanostructures that have been reported, metal-tipped semiconductor nanorods are perhaps the most intensively studied, and their use as a photocatalyst will be the focus of the chapter. First, we will discuss different wet-chemical synthesis techniques to control the synthesis of these metal–semiconductor hybrid structures. Afterward, we will discuss their unique physicochemical properties that are a combination of semiconductor and metal properties. Finally, we will showcase several examples from the literature demonstrating the possible application of these unique hybrid structures in photocatalysis.

Keywords: semiconductor nanocrystals, metal–semiconductor, hybrid structures, charge separation, photocatalysis

1. Introduction

There has recently been great interest in metal-hybrid semiconductor nanoparticles. This is largely due to the fact that they can exhibit the physical and chemical characteristics of both the individual metal and semiconductor or display unique properties not seen in either component [1]. These hybrid materials can potentially be exploited for a number of applications which cannot be addressed by semiconductor-only particles, for example, the directed assembly of gold-tipped semiconductor nanorods where the gold tip acts as both a means to initiate directed assembly as well as serve as electrical contacts [2]. Most importantly, metal-tipped semicon-

ductors were found to be good photocatalysis, as shown by Costi et al., where redox-based reactions were enhanced by the fact that photogenerated charges in the semiconductor component could be transferred to the metal tip [3]. Such hybrid nanostructures combine different material components into a single nanoparticle and provide a powerful strategy for modifying the properties of nanoparticles. Colloidal metal-tipped semiconductor hybrid nanomaterials were first realized by Banin's group in 2004, where they demonstrated that gold nanocrystals preferentially nucleate and grow at the tips of CdSe nanorods rather than at the sides of the nanorods (**Figure 1**) [4, 5]. These synthetic techniques opened up new possibilities for designing hybrid structures via epitaxial growth between a noble metal and semiconductors in colloidal solution. This can be seen in **Figure 2**, where TEM images are shown for a few hybrid structures, including Au–CdSe [6, 7], Au–ZnSe [8], Au–Bi_2S_3 [9], Au–SnS [10], and Au–CZTS [11].

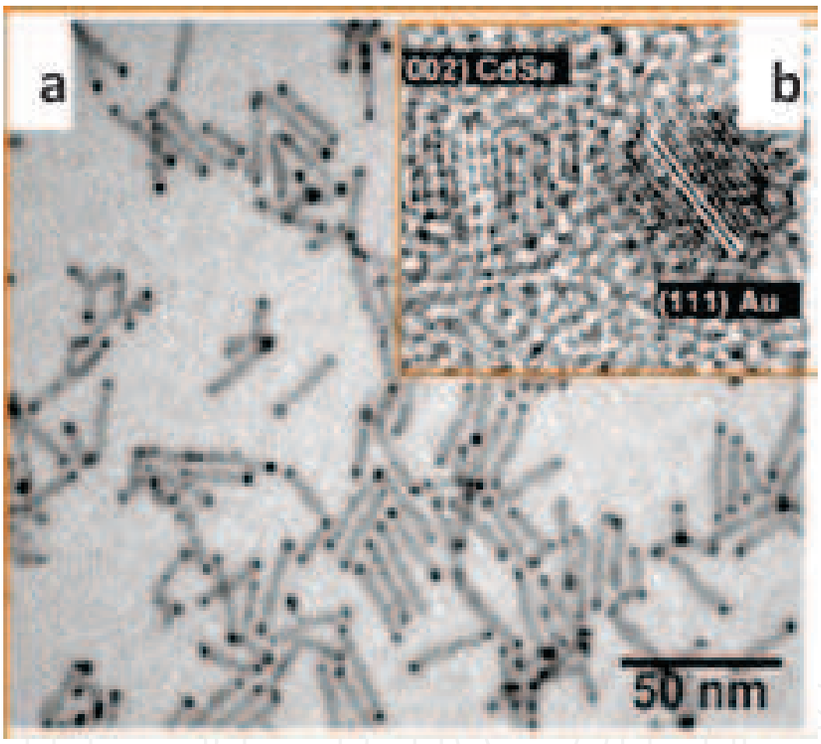

Figure 1. (a) CdSe nanorods after Au treatment using $AuCl_3$; Au tips are visible. (b) Inset shows HRTEM images of a single Au-tipped CdSe nanorod. The CdSe lattice for the rod in the center and Au tips at the rod edges can be identified, as marked. Adapted with permission [3].

Photocatalysis is a phenomenon in which photons are used for catalytically activating chemical reactions on the surface of photosensitized catalysts. Photocatalysis has been the hottest topic of research in the field of solar energy harvesting [9, 13–17]. In these processes, the photocatalyst generates charge carriers upon excitation from a suitable light source. These photoexcited charges are then transferred to reaction medium to initiate the chemical reaction. Over the decades, lots of progress has been made in photocatalysis research where researchers are using optically tuned semiconducting nanomaterials [18–21] and plasmonic noble metals [22–

http://dx.doi.org/10.5772/62636

24] as the photocatalyst. These materials have tunable absorption across the solar spectrum and can generate photoelectrons for use in a variety of chemical reactions. However, recent research efforts focused on using metal–semiconductor hybrid materials as a photocatalyst for harvesting solar energy show better results and will potentially opens up new avenues for photocatalysis [4, 11, 12, 25–31].

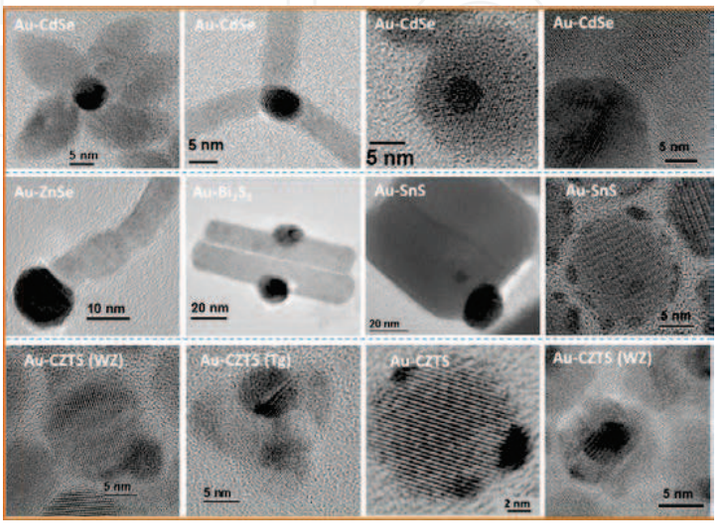

Figure 2. Representative HRTEM images of various nano-heterostructures. Reprinted with permission [12].

These metal–semiconductor hybrid materials can exhibit the properties of the individual materials or generate new properties when they combined together in the same nanostructures. In an ideal scenario, photogenerated charges could be quickly transferred to one component of the hybrid to the other due to band alignments, thus reducing the possibility of radiative recombination processes and enabling the opportunity for their use in chemical reactions [1, 4, 11, 27, 30]. In addition to that, these hybrid structures, because they can be engineered to have many different facets on their surface, have a higher probability for absorbing the targeted molecule of interest for photocatalytic conversion [1, 32]. In light of these unique properties, these metal–semiconductor hybrid structures have gained more attention for their use as photocatalysts as compared with the individual components.

The metal–semiconductor hybrid-based photocatalytic materials can be classified into three categories. In the first scenario, one of the components of the hybrid structure is the photoactive material, whereupon photo-excitation, the charge created transfers to the other component to start the catalytic process. An example of this category is the Au–TiO_2 hybrid structure, where gold act as a plasmonic antenna that absorbs light and generates charges, and the photo-excited plasmonic charges are then transferred to the higher bandgap TiO_2 [22, 26, 33–35]. This phenomenon can be illustrated in **Figure 3a**, where electrons from the surface plasmon state of Au are transferred to the higher bandgap material [36, 37]. In the second scenario, photo-excited electrons generated in low bandgap semiconductor nanoparticles transfer to the metal that it is attached to. Au–CdSe, Au–CdS, Au–PbS fall in this category, and a schematic is shown in **Figure 3b** [1, 32, 38, 39]. In the third scenario, as shown in **Figure 3c**, the coupling occurs

between excitons in the semiconductor and plasmons in gold [38, 40]. The excited state electronic coupling between two materials generates a greater number of charges and thus could be more effective for photocatalysis as compared with other two cases.

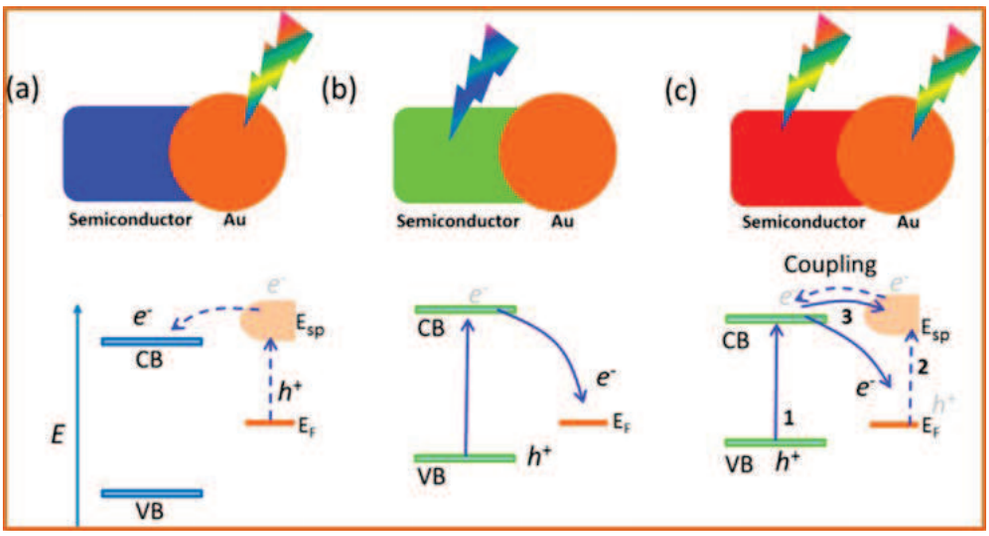

Figure 3. Schematic presentation of the electron transfer processes in Au-semiconductor heterostructures. For Au-semiconductor heterostructure where (a) only Au is excited, (b) only semiconductor is excited, and (c) there are simultaneous excitations of both Au and semiconductor. The electron transfer path 1 refers for semiconductor excitation followed by electron transfer to Au, path 2 follows just the reverse process, and path 3 shows the coupling of exciton of the semiconductor and plasmon of Au. Here, E_{sp} refers to the Au surface plasmon state and EF refers to the Au Fermi level. Adapted with permission [12].

This chapter will address the development of colloidal syntheses of hybrid metal–semiconductor nanocrystals and their application in the field of photocatalysis. Despite the plethora of examples of different-shaped metal–semiconductor nanostructures reported, metal-tipped semiconductor nanorods are perhaps the most intensively studied, and their uses as a photocatalyst will be the focus of the chapter. First, we will discuss different wet-chemical synthetic techniques to control the synthesis of these kinds of metal–semiconductor hybrid structures. Afterward, we will discuss their unique physicochemical properties that are a combination of both semiconductor and metal properties. And finally, we will showcase several examples from the literature, and how a researcher would use this unique hybrid structure for photocatalysis. The control over the synthesis of hybrid materials is among the hottest topic in the area of colloidal semiconductor nanocrystals or quantum dots (QDs) research. The metal–semiconductor hybrid materials are garnering lots of attention within the scientific community due to their unique properties primarily because these materials show size-dependent optical properties along with plasmonic properties of metals. In this chapter, we will highlight the following topics in detail:

1. Controlled synthesis of advanced metal–semiconductor hybrid materials.
2. Synergistic properties of metal–semiconductor hybrid materials.
3. Photocatalysis with metal–semiconductor hybrid materials.

http://dx.doi.org/10.5772/62636

2. Control synthesis of these advanced metal–semiconductor hybrid materials

After the first report of colloidal metal–semiconductor hybrid materials in 2004, the synthesis of these hybrid materials continues to develop rapidly. The synthesis process could be categorized in following ways. In Section 2.1, we will briefly discuss selective metal deposition onto semiconductors with the help of its different facets reactivity. In Section 2.2, we will see the synthesis of more complex genus particles, where two different metals are grown onto a single semiconductor nanostructure.

2.1. Selective metal deposition onto the semiconductor component

Selective metal deposition onto semiconductor components has gained lots of interest among synthetic routes. This synthetic process occurs due to heterogeneous nucleation of secondary metal particles on host semiconductor nanocrystals. This process is very practical as the heterogeneous nucleation energy barrier is lower compared with homogeneous self-nucleation and leads to the formation of crystalline-phase metallic particles while retaining the crystallinity of the host semiconductor.

Moreover, selective metal deposition onto the host semiconductor be dictated by the crystal morphology, and surface capping provides different chemical reactivities for different facets of the semiconductor nanocrystal. This leads to selective metal deposition onto the semiconductor where a higher reactive facet allows the first nucleation, which is followed by a less reactive facet. One example is anisotropic CdSe/CdS; CdS nanorods have different reactivates for each of its ends facets, and thus, by carefully controlling the Au precursor concentration, one could produce one tip, two tip, and finally everywhere Au–CdS nanorod hybrid structures as can be seen in **Figure 4a–c** [41]. Analogously, following a similar selective Au deposition onto PbS, spherical nanocrystals have been reported as well [44]. Another possible way to achieve selective metal deposition is via defect-mediated growth, since defects have higher energy, this allowing feasible secondary nucleation [45, 46]. Electrochemical Ostwald ripening processes have been found to be another alternate way to achieve selective one-tip metal deposition onto semiconductor nanocrystals [5]. This electrochemical Ostwald ripening process occurs via similar principles as Ostwald ripening, where a small island of particles dissolves to fuel the growth of a larger island. In addition to that, here, the electrochemical ripening requires oxidation/reduction of the metal components. The post-synthesis intraparticle Ostwald ripening due to thermal annealing has also been found to be useful to achieve selective metal deposition, as it is shown in the case of CdSe nanorods [6].

So far, the literature regarding site-selective deposition has been demonstrated on CdSe, CdS, and CdSe/CdS core/shell nanorods with the deposition of various metals, including Au [3, 5, 41, 45, 47], Pt [42, 48, 49], PtCo [42], PtNi [42], Pd, Ag_2S [41], Co [50], PdO, and Pd_4S [51]. Thermal- or photochemical-assisted metal deposition can lead to the formation of different metallic patterns on to the semiconductor surface. This mainly depends on various factors, such as the selection of surface ligands, metal precursor concentration, and reaction temperature. For example, high temperature leads to the formation of facet selective Pt deposition on

CdS nanorods (**Figure 4e**) [42], whereas photodeposition of Pt onto CdS favors no selectivity [48]. On the contrary, hierarchical one tip, two tip, and everywhere Au deposition onto CdSe/CdS nanorod was demonstrated to depend on Au precursor concentration [41]. Similarly, selective photodeposition of Pd nanoparticles onto $CdS_{0.4}Se_{0.6}$ nanorods were also reported [52]. The selective metal deposition onto semiconductor branched structures such as CdSe/CdS tetrapods was difficult to achieve due to the similar reactivity of all four arm tips. Recently, we overcome this problem by controlling the surface morphology of the CdSe/CdS tetrapods with the use of surface capping groups. The selective metal deposition was demonstrated in the cone-like tapered CdSe/CdS tetrapod which has increased selectivity towards single Au tipped (**Figure 4g**) [43]. The rectangular-shaped tetrapods do not show (Figure 4h) any such selectivity, and gold deposition occurs everywhere onto the CdS surface [43]. This unusual metal deposition was attributed to the intraparticle electrochemical Ostwald ripening process.

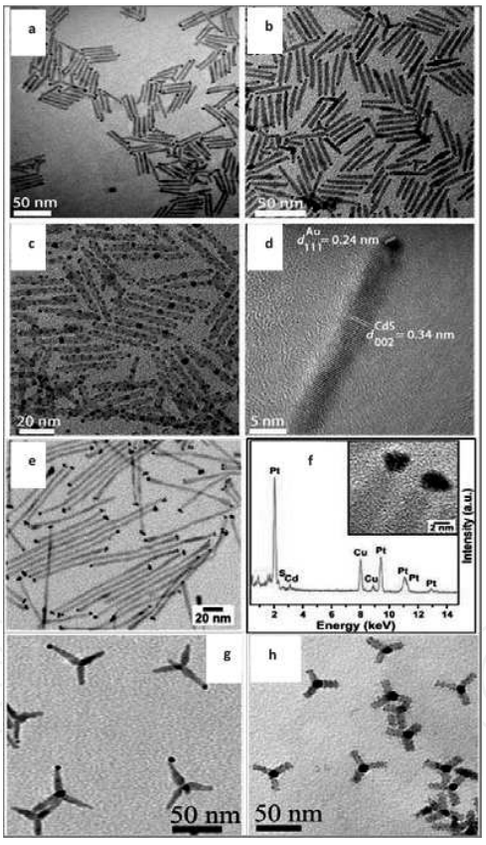

Figure 4 TEM images of CdSe-seeded CdS nano-heterostructures with controlled, varying degrees of Au deposition: CdSe/CdS nanorods exposed to increasing concentrations of Au precursor, resulting in Au deposited at (a) one end, (b) both ends, and (c) throughout the rod, respectively; (d) HRTEM image showing a gold nanoparticle at the apex of the nanorod. The measured d-spacing values from the visible lattice fringes 0.24 and 0.34 nm are assigned to Au (111) and CdS (002), respectively. (e) CdS with small single Pt tips (4.3 nm). (f) Selected area EDS spectrum of a single Pt tip, with inset HRTEM image of two Pt–CdS hybrids. (g, h) TEM images of tetrapods exposed to high concentrations of Au precursor. All of the reactions were done at room temperature for a fixed reaction time of 1.5 h. Adapted with permission [41–43].

http://dx.doi.org/10.5772/62636

2.2. Genus hybrid nanoparticles (semiconductor–dual metal) via selective deposition

Incorporating more than one metal particle onto semiconductor nanocrystals could produce genus type of hybrid material with new chemical and physical properties. This could be achieved via core/shell structures where one metal acts as core for another metal or through interfacial alloying. It was reported previously that bimetallic nanocrystals could enhance the photocatalytic performance [53]. In the case of Pt/Ni and Pt/Ru/Ni alloy nanoparticles, it was found that they show improved catalytic performance compared with pure Pt nanoparticles [54].

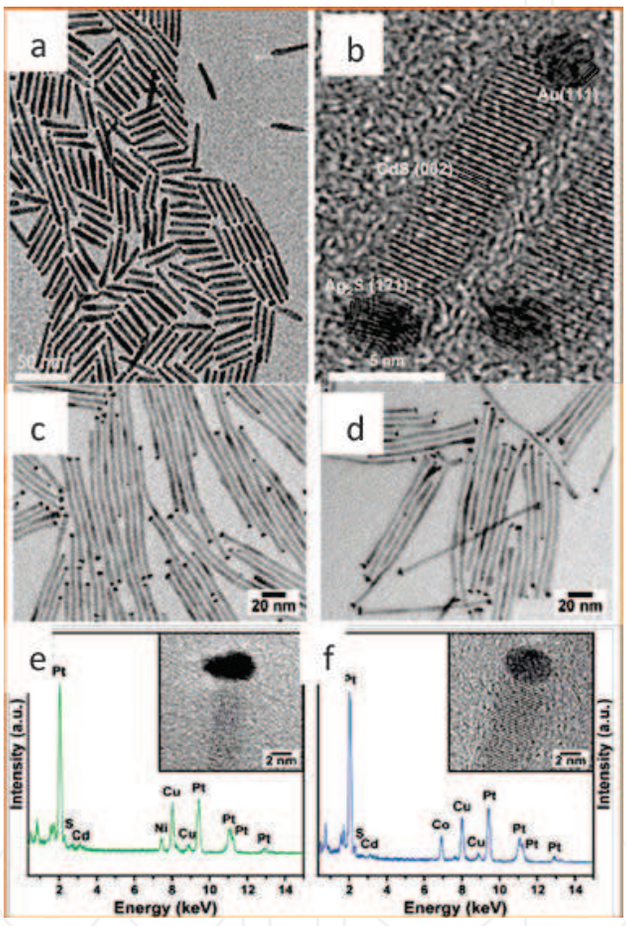

Figure 5. (a) TEM image of seeded CdSe/CdS nanorods with Au nanoparticles at one end and Ag_2S nanoparticles at the other end. (b) HRTEM image showing the visible lattice fringes of the Ag_2S {1¯21} and Au {111} planes with measured d-spacings of 0.26 and 0.24 nm, respectively. (c, d) TEM images of binary-CdS heterostructure nanoparticles with different sizes and ompositions: (c) PtNi–CdS (4.7 nm), (d) PtCo–CdS (5.2 nm), prepared with increased metal concentration showing a loss of selectivity, (e) selected area EDS spectrum taken on the tip of a PtNi–CdS hybrid structure, (f) selected area EDS spectrum of a PtCo–CdS heterostructure. Adapted with permission [41, 42].

In the recent work, using two different metal precursors in the growth solution, Habas et al. [42] reported the synthesis of genus hybrid materials such as CdS–PtNi and CdS–PtCo, in which metals formed an interfacial alloy (**Figure 5c, d**). Afterward, Chakrabortty et al. [41] reported Au–CdSe/CdS–Ag_2S types of genus particles with selective metal deposition using

the difference of reactivity between the two tips of CdSe/CdS rods (**Figure 5a, b**). Moreover, our recent work shows the one Au-tipped CdSe/CdS tetrapods could be useful for further growth of a second metal (Ag in this case) onto the other three CdS tips, as described by schematic in **Figure 6a** [43]. The TEM image in the **Figure 6b** shows the genus structures where one tip of the tetrapod structures has Au and other three have Ag_2S. Further confirmation was done with the HRTEM analysis of single particle which confirms lattice fringes of both Au and Ag_2S (**Figure 6d, e**). Another approach used was light-induced deposition of a secondary metal onto CdSe/CdS–Au hybrid nanorods [55]. UV irradiation causes the exciton to be formed in the CdSe/CdS semiconductor nanorod, and charge separation does occur due to the presence of the Au tip which serves as an electron sink. These electrons reach the Au tips and then act as reduction point for the second metal ions, such as Pd or Fe, and form hybrid genus particles with alloyed Pd/Au tips or Au/Fe_xO_y hollow core/shell structures, which can be seen in **Figure 7a, b** [55]. With the help of kinetically controlled syntheses, Hill et al. reported selective deposition of Co and Co_xO_y on Pt-tipped CdSe/CdS core/shell nanorods (**Figure 7c–h**) [56].

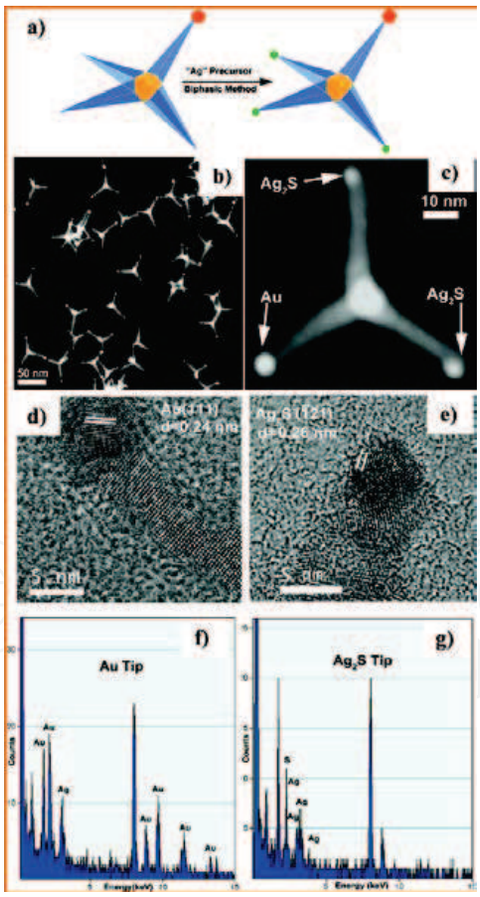

Figure 6. (a) Reaction schematic to obtain hierarchically complex CdSe-seeded CdS tetrapods with Au at precisely one tip and Ag_2S at the other three. (b) Representative HAADF-STEM image of tetrapods with cone-like arms fabricated according to the strategy shown in a. (c) Magnified view of one of the tetrapods in b, with the different tips labeled. (d, e) HRTEM images of the different tetrapod arm tips showing the visible lattice fringes of the Ag_2S (1⊚21) and Au (111)

http://dx.doi.org/10.5772/62636

planes with measured d-spacings of 0.26 and 0.24 nm, respectively. Further confirmation of the (f) Au and (g) Ag_2S tip elemental composition by EDX, respectively. Adapted with permission [43].

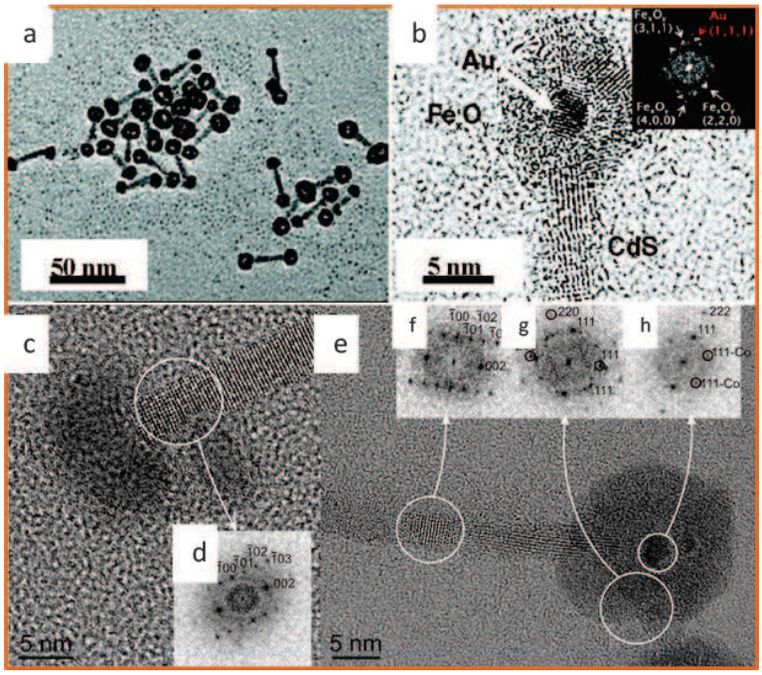

Figure 7. (a) TEM image of ~2.8 nm diameter core Au nanoparticles with a ~3.3 nm thick hollow shell of Fe_xO_y exclusively at the Tips of 29 nm long CdSe-seeded CdS semiconductor nanorods. (b) HRTEM image of part of the core-shell-tipped rod. The inset is an FFT image of the spherical tip region. HRTEM and power spectrum analysis used to determine the crystalline phases in (core@shell) (c, d) Pt@Co-tipped and (e, f) Pt@CoO-tipped nanorods. Nanorod dimensions: L = 40 nm, cobalt diameter: D = 12 nm. Adapted with permission [55, 56].

3. Synergistic properties of metal–semiconductor hybrid materials

Metal–semiconductor hybrid materials show some unique properties that arise from the combination of the two different materials on a single particle. Next, we will discuss these properties of hybrid materials, starting with the optical properties (Section 3.1), followed by charge separation in these structures (Section 3.2).

3.1. Optical properties

Metal-tipped semiconductor and core/shell metal–semiconductor hybrid structures show absorption spectra exhibiting combined coupling effects that cannot be replicated with a simple physical mixture of both components. In these hybrid structures, strong coupling occurs between the electronic states of metal and semiconductor, which leads to broadening and shifts in the plasmonic peak of the metal [57] and the excitonic absorption peak of the semiconductor [47]. This could be as a result of the formation of new electronic states in the semiconductor–metal interface. The electrodynamic effect could be another possible reason for the formation of new features in the absorption spectra [58]. The spectra in **Figure 8a, b**

show similar changes in the plasmonic shift occurring in Au–CZTS and Au–Bi_2S_3 hybrid nanostructures [9, 10]. Due to the coupling of Au plasmons with semiconductor excitons, a strong optical field is generated at the interface of Au. This coupling could be the key factor for the suppression of the exciton, which is facilitated by the efficient transfer of the electrons for triggering photocatalytic chemical reactions. Figure 8c shows Au–CdS hybrid structures, which exhibit both the characteristic excitonic and continuous absorption of the CdS nanorods below 475 nm and an additional broad absorption centered around 532 nm due to the plasmonic Au [38].

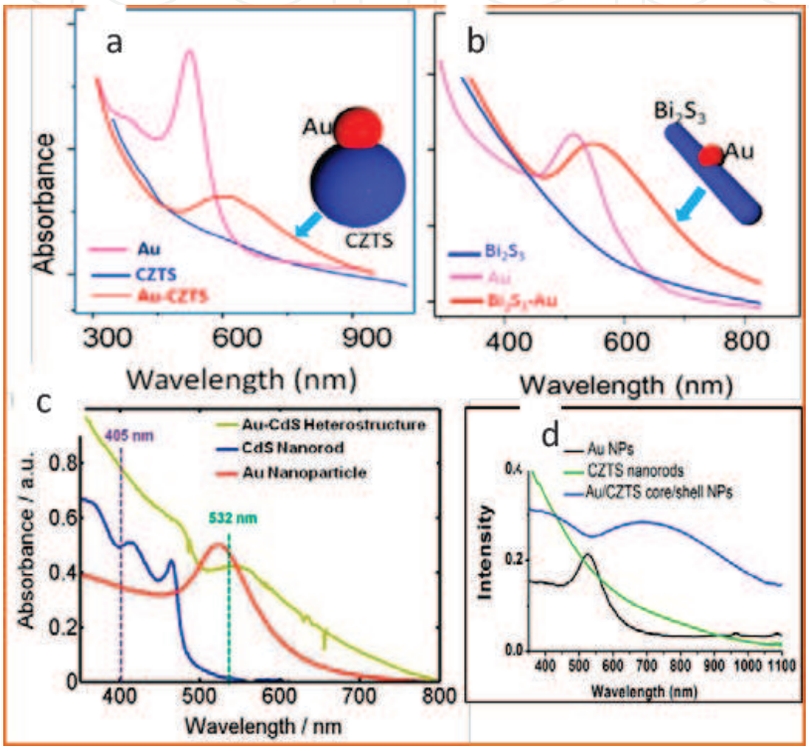

Figure 8. Absorption spectra of (a) Au, CZTS, and coupled Au–CZTS heterostructure and of [10]. (b) Au, Bi_2S_3, and Au–Bi_2S_3 heterostructure [9]. (c) UV–Vis absorption spectra of pure CdS nanorods (blue curve), Au nanoparticles (red curve), and high Au–CdS heterostructures (10.8 wt%, yellow curve). The green- and purple-dotted lines indicate the excitation source of a 532 nm laser and a 405 nm laser, respectively [38]. (d) UV–Vis spectra of Au NPs (black), CZTS NPs (green), and Au/CZTS core/shell NPs (blue). Adapted with permission [31].

Figure 8d shows UV–Vis spectra of Au NPs, CZTS NPs, and Au/CZTS core/shell NPs [31]. The thick CZTS shell surrounding the Au cores causes the shift of the plasmonic peak of bare Au particles from 525 to 685 nm. The high dielectric constant of low bandgap CZTS to the composite materials could be the possible reason behind it. The core/shell Au/CZTS hybrid structures also exhibited a broadened peak between 570 and 1100 nm that is a result of the perturbation of energy states by the plasmonic field.

Additionally, these metal–semiconductor hybrids either enhance [59–61] or quench [41, 62] the fluorescence of the semiconductor. Enhancement of the semiconductor emission occurs due to plasmonic effects of metallic portion, but it is strongly dependent on the distance

http://dx.doi.org/10.5772/62636

between the metal and fluorescent semiconductor [63]. Direct growth of the metallic particle onto the semiconductor nanocrystals often exhibits quenching. The charge transfer from the excited semiconductor to the metal is the main cause behind fluorescence quenching thus reduced the radiative life time. This observation is common and can be seen in ZnO–Ag [64], CdS–Au [47], CdSe–Au [3], and CdTe–Au nanoparticles [65]. On the other hand, fluorescence enhancement is generally obtained when a spacer material is introduced in between the metal and semiconductor. One kind of this example is CdSe/ZnS nanoparticles adsorbed on an Ag/SiO_2 core/shell structure. By controlling the thickness of the SiO_2 shell, fluorescence enhancement has been observed with increased SiO_2 shell thickness and attributed to an excitation enhancement effect [66].

3.2. Photo-induced charge separation

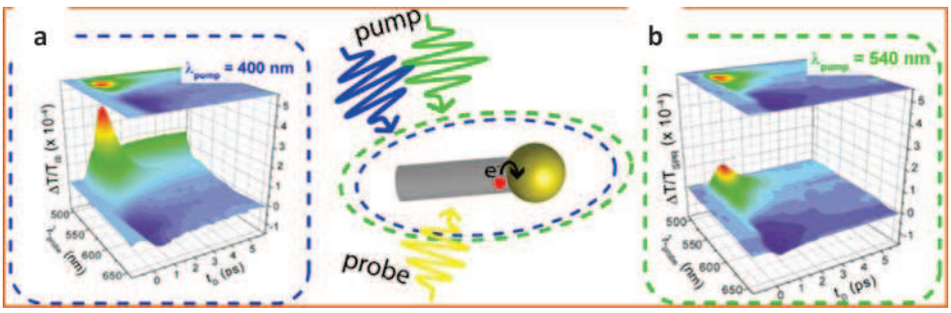

Figure 9. Ultrafast response of semiconductor–metal nanohybrids: Probing the Au nanoparticle spectral region. Time and spectrally resolved transmission change ΔT/T(tDprobe, λprobe) measured in CdS–Au nanomatchsticks solution for a pump wavelength (a) λpump = 400 nm [below the CdS bandgap and gold interband transition threshold: ΔT/TIB (b) λpump = 540 nm (close to the surface plasmon resonance of gold nanoparticles: ΔT/TSPR) and]. Adapted with permission [67].

Previous work reported the growth of metallic nanoparticles onto a semiconductor facilitates rapid charge transfer from the semiconductor to the metal particle upon light excitation, leading to charge separation [4, 9]. Due to the band alignment at the semiconductor/metal interface, the Fermi level of the metal component is located within the bandgap of the semiconductor, and electronic states promote the transfer of the excited electrons in the semiconductor conduction band into the metal energy levels. On the other hand, holes may remain localized to surface defect states in the semiconductor, or to confined levels, as may be in cases in type-II and quasi type-II core/shell structures. Mongin et al. [67] reported a study of the ultrafast photo-induced charge separation in single-tipped CdS–Au nanorods.

In this work, pump–probe measurements (schematic shown in **Figure 9**) were performed on the semiconductor and the metal domains separately, measuring the contribution of the photo-induced charge transfer. The spectral and amplitude changes between pump, having wavelength corresponding to the plasmonic of metal region, (Figure 9) and pump, having wavelength corresponding to the semiconductor absorption region, (Figure 9) are attributed to charge transfer. Reported transient absorption measurements on other hybrid materials including CdS–Pt [68, 69] and ZnSe/CdS–Pt [68] were interpreted as exhibiting longer charge

separation times such as 3–4 and 14 ps, respectively. The understanding of charge separation and exciton dynamics in these hybrid structures is the key factors for their application in photocatalysis, which is discussed in next section.

4. Photocatalysis with metal–semiconductor hybrid materials

One of the most interesting applications of these metal–semiconductor hybrid structures is photocatalysis. The combined properties make these hybrid structures efficient for photocatalysis. These types of colloidally synthesized hybrid materials work as heterogeneous photocatalysis. Efficient light energy conversion occurs which could be used for photodegradation of organic pollutants in water [70], in photo-electrochemical cells for energy storage [71], and for photo-induced water-splitting hydrogen generation [72]. With a judicious choice of two different components in a semiconductor–metal hybrid, one can tune the band alignment accordingly to match the reduction potential of the target system for photocatalysis. For example, semiconductor core/shell structures with type-II band alignment facilities the charge separation with long-lived excitons. Thus, a metal tip onto these type-II structures could easily extract the charge and act as reservoir of electrons. In addition to that, high crystalline quality in these hybrid structures is required for two reasons: (1) Surface defects localize the charges and reduce the photocatalytic efficiency, and (2) a less defective surface will also enhance the mobility [72]. Photocatalysis using these hybrid structures can be categorized in the following sub topics.

4.1. Photocatalytic redox reactions

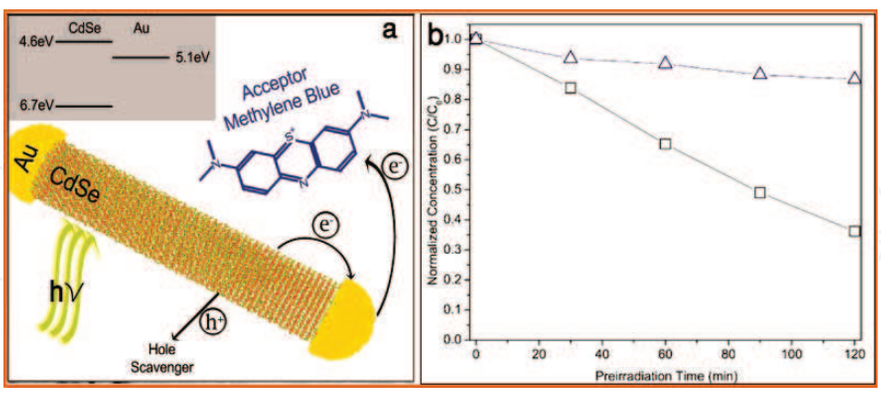

Figure 10. (a) Scheme of a light-induced charge separation mechanism in a nanodumbbell in which the photogenerated electron–hole pair separates so that the electron resides at the gold tip and the hole at the CdSe nanorod. The scheme also depicts the transfer of the hole to the scavenger and the reduction of the MB molecule upon electron transfer from the gold tip. The inset shows the energy band alignment between CdSe (4 nm dots) and Au. (b) Normalized concentration of MB dye reduced by CdSe nanorods gold nanoparticles mixture (open blue triangles) and by hybrid CdSe–Au nanodumbbells solution (open black squares) vs. pre-irradiation time. High efficiency of the charge retention in NDBs is demonstrated, leading to activity toward MB reduction. Adapted with permission [4].

http://dx.doi.org/10.5772/62636

Since the pioneering work by the Banin group using Au-tipped-CdSe rods for the reduction of the organic dye Methylene blue (MB) [4], several research groups demonstrated photocatalysis with different hybrid structures. In the work by the Banin group, they demonstrated proof of concept of charge separation due to the band alignment (see **Figure 10a**) between CdSe and Au. **Figure 10b** shows the degradation of the MB dye with CdSe–Au as a catalyst has more efficiency as compared with the Au particle/CdSe nanorod physical mixture [4]. Similar studies were found in the case of CdS–Au [38].

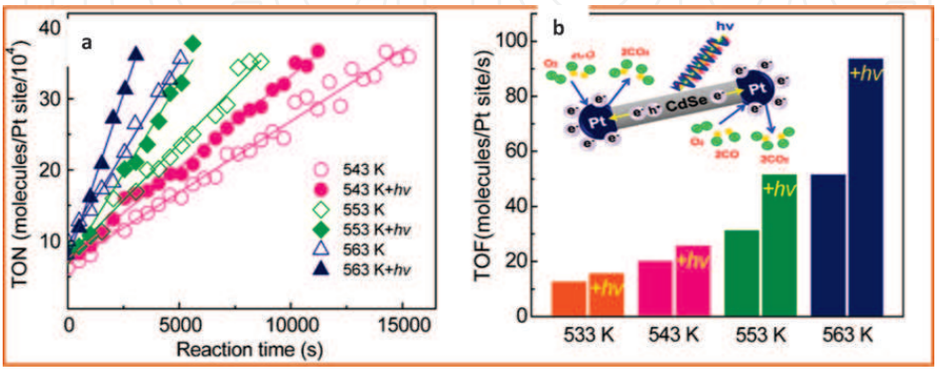

Figure 11. (a) Turnover number (TON) for CO oxidation on Pt–CdSe–Pt nanodumbbells with and without light at three different temperatures and (b) TOF for CO oxidation on Pt–CdSe–Pt nanodumbbells with and without light at four different temperatures. During CO oxidation, the TON was measured after a certain amount of time to allow for product molecules to accumulate. Time zero is the point when we started collecting data, not the start of the reaction. Adapted with permission [73].

Soon after, the first reports several research group work onto this hybrid system for photocatalysis application. Kim et al demonstrated [73] that hot carriers generated upon photon absorption in Pt–CdSe–Pt nanodumbbells significantly impact the catalytic activity of CO oxidation. They found that this hybrid structure exhibits a higher turnover frequency by a factor of 2 during irradiation by light with energy higher than the bandgap of CdSe

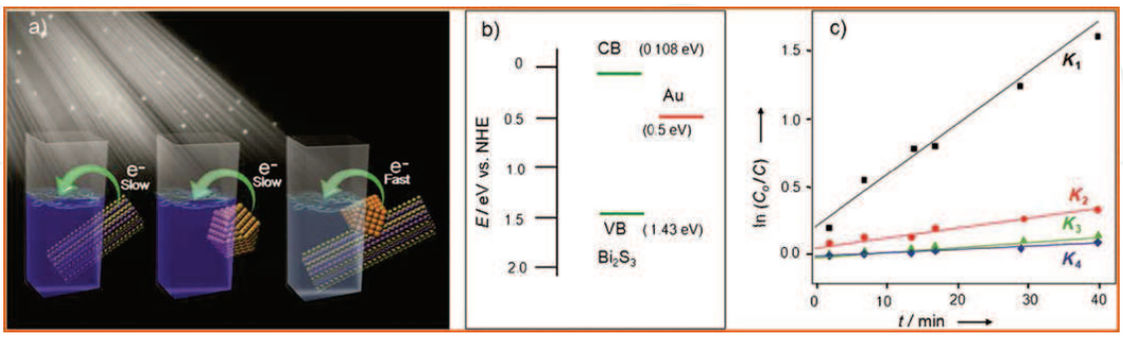

Figure 12. (a) Schematic representation of conditions for the favorable photoreduction of methylene blue. (b) Band alignment of Bi_2S_3 and Au (CB = conduction band, VB = valence band). (c) Rate of dye degradation with irradiation progress under different conditions. The samples were irradiated using Xe lamp with a wavelength of 500 nm. K1 (0.037 min_1), K2 (0.007 min_1), K3 (0.004 min_1), and K4 (0.002 min_1) are the dye degradation rate constants with Au–Bi_2S_3, a mixture of Au and Bi_2S_3, Bi_2S_3, and Au, respectively. Adapted with permission [9].

(**Figure 11a**), while the turnover rate on bare Pt nanoparticles did not depend on light irradiation. The Figure 11b shows enhanced catalytic activity as is demonstrated for the turnover frequency (TOF) under light irradiation at four different temperatures.

More recently, the Pradhan group demonstrated hybrid Au–Bi_2S_3 heterostructures exhibit photo-catalytic activity which is similar to CdS and CdSe systems [9]. The rate of MB reduction using Au-Bi_2S_3 is shown in **Figure 12c**. Au–SnS is another new hybrid material developed by same group, and it also shows enhancement of the rate of catalytic activities in the reduction of the dye MB compared with only SnS nanocrystals [10].

4.2. Photocatalytic water splitting

Photocatalytic water splitting for hydrogen generation using these hybrid structures has also gained lot of attention [11, 31]. In this process, the photo-excited electron reduces the H^+ ions to molecular H_2. Amirav et al. [74] demonstrated that in the case for CdSe/CdS–Pt nanorods,

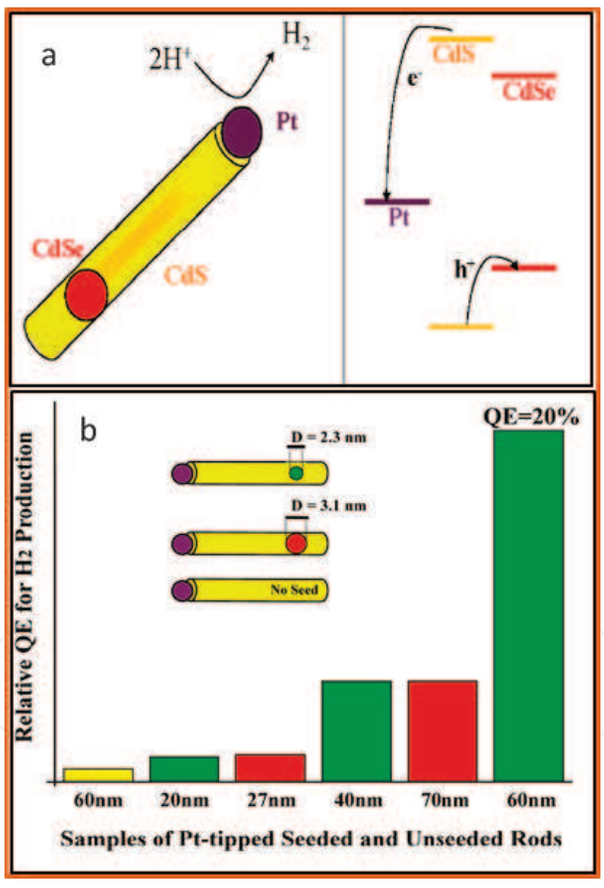

Figure 13. (left top corner) An illustration of the multicomponent nano-heterostructure, composed of a Pt-tipped CdS rod with an embedded CdSe seed. (Top middle) An illustration of the energy band diagram indicating that holes are confined to the CdSe, while electrons are transferred to the Pt and are thus separated from the holes (B) relative quantum efficiency for hydrogen production, obtained from platinum-tipped unseeded CdS rods (yellow), and five different samples of platinum-tipped seeded rods, with seed diameters of 3.1 (red) or 2.3 nm (green). Underneath each bar is the corresponding average sample length. Adapted with Permission [74].

http://dx.doi.org/10.5772/62636

the longer rods provided higher hydrogen production due to better spatial charge separation along the rod length and reduced back-recombination. **Figure 13b** shows the length dependence and effect of core/shell nanorods on the hydrogen production yield. The long arm core/shell CdSe/CdS–Pt hybrid structures have the highest production yield. Additionally, between the two different core/shell CdSe/CdS–Pt hybrid structures, the smaller CdSe core shows higher hydrogen production, because the smaller CdSe core forms quasi type-II band alignment upon growing the CdS rod-like shell over it and thus facilitates charge separation.

Another recent example by Ha et al. shows core/shell hybrid structures with Au core and CZTS shell (**Figure 14a**) could be useful for water splitting (**Figure 14b**) [31]. The CZTS band alignment with respect to Au Fermi level facilities the faster transfer of the photogenerated charge carriers. The S^{2-}/SO_3^{2-} solution acts as a hole scavenger during the photocatalytic process while core/shell structures are more efficient than other shapes of CZTS nanostructures. In this particular example, Au is located at the core, it is expected that upon photo-excitation, and both the electron and hole are transferred to the conduction and valence bands of CZTZ. Therefore, this structure is superior in terms of charge separation for photocatalytic water splitting.

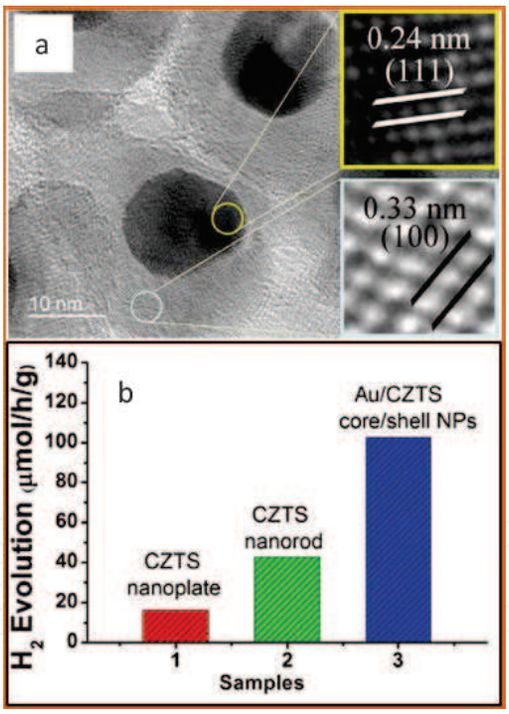

Figure 14. (a) Typical TEM and high-resolution TEM image of as-prepared Au/CZTS core/shell NPs. (b) A Plot comparing the photocatalytic H_2 evolution among CZTS nanoplates (red), CZTS nanorods (green), and Au/CZTS core/shell NPs (blue). Adapted with permission [31].

Another example is demonstrated by Cabot et al. [11] where they examined the activity of CZTS, CZTS–Au, and CZTS–Pt toward photocatalytic hydrogen evolution from water splitting. Interestingly, they found Pt-tipped CZTS is better as compared with Au tipped (**Figure 15c**), where both the hybrid structures are dramatically better than CZTS alone. Here,

the authors used Na_2S and Na_2SO_3 were used as hole scavengers. According to their observation, CZTS–Pt provided the highest H_2 evolution rate (1.02 mmol/g h), which was eightfold higher than that of bare CZTS (0.13 mmol/g·h) and 1.25 times than CZTS–Au. The reasons for high efficiency in the case of CZTS–Pt were not explained well by the authors.

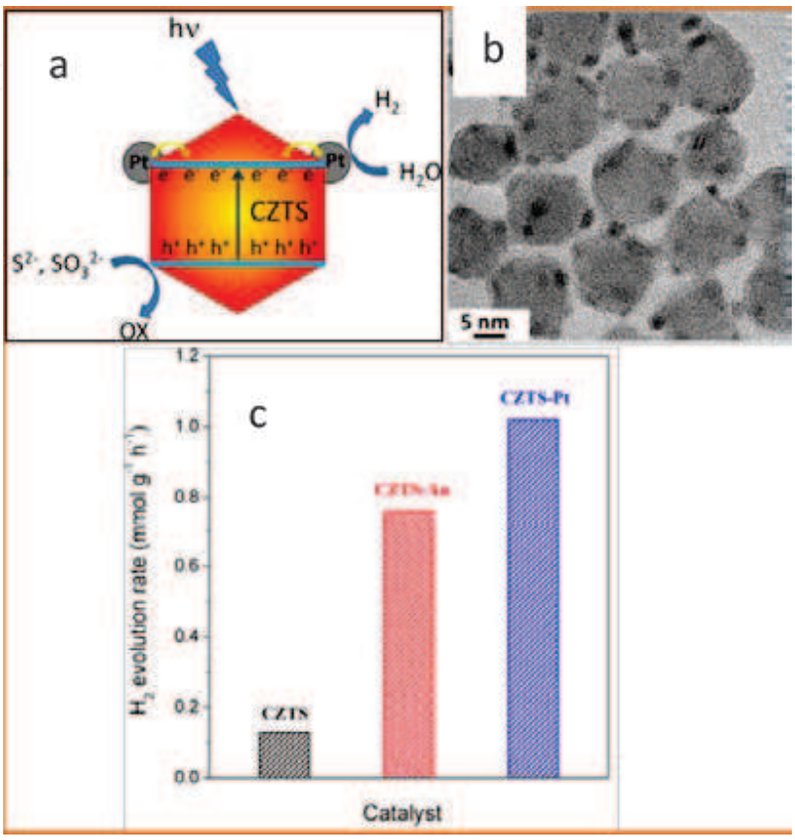

Figure 15. (a) Illustration of the possible mechanism of enhancement of the H_2 evolution rate in CZTS–Pt. (b) HR TEM image of CZTS–Pt heterostructured nanoparticles. (c) Hydrogen evolution rate of CZTS, CZTS–Au, and CZTS–Pt nanomaterials during a 4 h test. Adapted with permission [11].

5. Conclusion

In the last decade, substantial advancements have been made with selective metal deposition onto different-shaped semiconductor nanocrystals. The control synthesis has been demonstrated from binary to ternary hybrid materials with more than one metal onto semiconductor having multiple functionalities. The degree of control was achieved in terms of selective metal deposition onto branched semiconductor structures. An effort has been made in order to understand the fundamentals of the synergistic properties of these special materials related to nonconventional material combinations. Furthermore, few studies were done of light-induced charge separation at the semiconductor–metal interface, which serves as a basis for the implementation of these hybrid structures in photocatalysis applications. In coming

years, further understanding of photo-induced charge separation at the metal semiconductor interface is also expected to develop. Thus, the path for unique applications of these hybrid systems in the field of photocatalysis will further develop in coming years. Future syntheses of metal/semiconductor hybrid structures will yield a wide range of materials for different applications, including practical application in photocatalysis and electronic devices.

Author details

Nimai Mishra

Address all correspondence to: nimaiiitm@gmail.com

CINT—Center for Integrated Nanotechnologies, Los Alamos National Laboratory, Los Alamos, USA

References

[1] Costi, R.; Saunders, AE; Banin, U. Colloidal Hybrid Nanostructures: A New Type of Functional Materials. *Angew. Chem. Int. Ed.* 2010, *49* (29), 4878–4897.

[2] Zhao, N.; Liu, K.; Greener, J.; Nie, Z.; Kumacheva, E. Close-Packed Superlattices of Side-by-Side Assembled Au-Cd Se Nanorods. *Nano Lett.* 2009, *9* (8), 3077–3081.

[3] Mokari, T.; Rothenberg, E.; Popov, I.; Costi, R.; Banin, U. Selective Growth of Metal Tips onto Semiconductor Quantum Rods and Tetrapods. *Science* 2004, *304* (5678), 1787–1790.

[4] Costi, R.; Saunders, AE; Elmalem, E.; Salant, A.; Banin, U. Visible Light-Induced Charge Retention and Photocatalysis with Hybrid CdSe–Au Nanodumbbells. *Nano Lett.* 2008, *8* (2), 637–641.

[5] Mokari, T.; Sztrum, CG; Salant, A.; Rabani, E.; Banin, U. Formation of Asymmetric One-Sided Metal-Tipped Semiconductor Nanocrystal Dots and Rods. *Nat. Mater.* 2005, *4* (11), 855–863.

[6] Figuerola, A.; van Huis, M.; Zanella, M.; Genovese, A.; Marras, S.; Falqui, A.; Zandbergen, HW; Cingolani, R.; Manna, L. Epitaxial CdSe–Au Nanocrystal Heterostructures by Thermal Annealing. *Nano Lett.* 2010, *10* (8), 3028–3036.

[7] Haldar, KK; Pradhan, N.; Patra, A. Formation of Heteroepitaxy in Different Shapes of Au–CdSe Metal–Semiconductor Hybrid Nanostructures. *Small.* 2013, *9* (20), 3424–3432.

[8] Bose, R.; Wasey, AHMA; Das, GP; Pradhan, N. Heteroepitaxial Junction in Au–ZnSe Nanostructure: Experiment Versus First-Principle Simulation. *J. Phys. Chem. Lett.* 2014, *5* (11), 1892–1898.

[9] Manna, G.; Bose, R.; Pradhan, N. Photocatalytic Au–Bi_2S_3 Heteronanostructures. *Angew. Chem.* 2014, *126* (26), 6861–6864.

[10] Patra, BK; Guria, AK; Dutta, A.; Shit, A.; Pradhan, N. Au-SnS Hetero Nanostructures: Size of Au Matters. *Chem. Mater.* 2014, *26* (24), 7194–7200.

[11] Yu, X.; Shavel, A.; An, X.; Luo, Z.; Ibáñez, M.; Cabot, A. Cu_2ZnSnS_4-Pt and Cu_2ZnSnS_4-Au Heterostructured Nanoparticles for Photocatalytic Water Splitting and Pollutant Degradation. *J. Am. Chem. Soc.* 2014, *136* (26), 9236–9239.

[12] Dutta, SK; Mehetor, SK; Pradhan, N. Metal Semiconductor Heterostructures for Photocatalytic Conversion of Light Energy. *J. Phys. Chem. Lett.* 2015, *6* (6), 936–944.

[13] Maeda, K.; Domen, K. Photocatalytic Water Splitting: Recent Progress and Future Challenges. *J. Phys. Chem. Lett.* 2010, *1* (18), 2655–2661.

[14] Zhao, J.; Osterloh, FE Photochemical Charge Separation in Nanocrystal Photocatalyst Films: Insights from Surface Photovoltage Spectroscopy. *J. Phys. Chem. Lett.* 2014, *5* (5), 782–786.

[15] Liao, L.; Zhang, Q.; Su, Z.; Zhao, Z.; Wang, Y.; Li, Y.; Lu, X.; Wei, D.; Feng, G.; Yu, Q.; Cai, X.; Zhao, J.; Ren, Z.; Fang, H.; Robles-Hernandez, F.; Baldelli, S.; Bao, J. Efficient Solar Water-Splitting Using a Nanocrystalline CoO Photocatalyst. *Nat. Nanotechnol.* 2014, *9* (1), 69–73.

[16] Khon, E.; Lambright, K.; Khnayzer, RS; Moroz, P.; Perera, D.; Butaeva, E.; Lambright, S.; Castellano, FN; Zamkov, M. Improving the Catalytic Activity of Semiconductor Nanocrystals Through Selective Domain Etching. *Nano. Lett.* 2013, *13* (5), 2016–2023.

[17] Kamat, PV Manipulation of Charge Transfer Across Semiconductor Interface. A Criterion That Cannot Be Ignored in Photocatalyst Design. *J. Phys. Chem. Lett.* 2012, *3* (5), 663–672.

[18] Trotochaud, L.; Mills, TJ; Boettcher, SW An Optocatalytic Model for Semiconductor–Catalyst Water-Splitting Photoelectrodes Based on In Situ Optical Measurements on Operational Catalysts. *J. Phys. Chem. Lett.* 2013, *4* (6), 931–935.

[19] Ma, SSK; Hisatomi, T.; Maeda, K.; Moriya, Y.; Domen, K. Enhanced Water Oxidation on Ta_3N_5 Photocatalysts by Modification with Alkaline Metal Salts. *J. Am. Chem. Soc.* 2012, *134* (49), 19993–19996.

[20] Maeda, KZ-Scheme Water Splitting Using Two Different Semiconductor Photocatalysts. *ACS Catal.* 2013, *3* (7), 1486–1503.

[21] Martin, DJ; Qiu, K.; Shevlin, SA; Handoko, AD; Chen, X.; Guo, Z.; Tang, J. Highly Efficient Photocatalytic H2 Evolution from Water Using Visible Light and Structure-Controlled Graphitic Carbon Nitride. *Angew. Chem. Int. Ed.* 2014, *53* (35), 9240–9245.

[22] Linic, S.; Christopher, P.; Ingram, DB Plasmonic-Metal Nanostructures for Efficient Conversion of Solar to Chemical Energy. *Nat. Mater.* 2011, *10* (12), 911–921.

[23] Zheng, Z.; Tachikawa, T.; Majima, T. Single-Particle Study of Pt-Modified Au Nanorods for Plasmon-Enhanced Hydrogen Generation in Visible to Near-Infrared Region. *J. Am. Chem. Soc.* 2014, *136* (19), 6870–6873.

[24] Zhang, L.; Kim, HY; Henkelman, G. CO Oxidation at the Au–Cu Interface of Bimetallic Nanoclusters Supported on CeO2(111). *J. Phys. Chem. Lett.* 2013, *4* (17), 2943–2947.

[25] Ingram, DB; Linic, S. Water Splitting on Composite Plasmonic-Metal/Semiconductor Photoelectrodes: Evidence for Selective Plasmon-Induced Formation of Charge Carriers near the Semiconductor Surface. *J. Am. Chem. Soc.* 2011, *133* (14), 5202–5205.

[26] DuChene, JS; Sweeny, BC; Johnston-Peck, AC; Su, D.; Stach, EA; Wei, WD Prolonged Hot Electron Dynamics in Plasmonic-Metal/Semiconductor Heterostructures with Implications for Solar Photocatalysis. *Angew. Chem. Int. Ed.* 2014, *53* (30), 7887–7891.

[27] Jakob, M.; Levanon, H.; Kamat, PV Charge Distribution between UV-Irradiated TiO2 and Gold Nanoparticles: Determination of Shift in the Fermi Level. *Nano. Lett.* 2003, *3* (3), 353–358.

[28] Li, J.; Cushing, SK; Zheng, P.; Senty, T.; Meng, F.; Bristow, AD; Manivannan, A.; Wu, N. Solar Hydrogen Generation by a CdS–Au–TiO2 Sandwich Nanorod Array Enhanced with Au Nanoparticle as Electron Relay and Plasmonic Photosensitizer. *J. Am. Chem. Soc.* 2014, *136* (23), 8438–8449.

[29] Subramanian, V.; Wolf, E.; Kamat, PV Semiconductor–Metal Composite Nanostructures. To What Extent Do Metal Nanoparticles Improve the Photocatalytic Activity of TiO2 Films? *J. Phys. Chem. B* 2001, *105* (46), 11439–11446.

[30] Banin, U.; Ben-Shahar, Y.; Vinokurov, K. Hybrid Semiconductor–Metal Nanoparticles: From Architecture to Function. *Chem. Mater.* 2014, *26* (1), 97–110.

[31] Ha, E.; Lee, LYS; Wang, J.; Li, F.; Wong, K-Y; Tsang, SCE Significant Enhancement in Photocatalytic Reduction of Water to Hydrogen by Au/Cu_2ZnSnS_4 Nanostructure. *Adv. Mater.* 2014, *26* (21), 3496–3500.

[32] Sheldon, MT; Trudeau, P-E; Mokari, T.; Wang, L-W; Alivisatos, AP Enhanced Semiconductor Nanocrystal Conductance via Solution Grown Contacts. *Nano Lett.* 2009, *9* (11), 3676–3682.

[33] Xing, M-Y; Yang, B-X; Yu, H.; Tian, B-Z; Bagwasi, S.; Zhang, J-L; Gong, X-Q Enhanced Photocatalysis by Au Nanoparticle Loading on TiO2 Single-Crystal (001) and (110) Facets. *J. Phys. Chem. Lett.* 2013, *4* (22), 3910–3917.

[34] Subramanian, V.; Wolf, EE; Kamat, PV Catalysis with TiO2/gold Nanocomposites. Effect of Metal Particle Size on the Fermi Level Equilibration. *J. Am. Chem. Soc.* 2004, *126* (15), 4943–4950.

[35] Farnesi Camellone, M.; Marx, D. On the Impact of Solvation on a Au/TiO2 Nanocatalyst in Contact with Water. *J. Phys. Chem. Lett.* 2013, *4* (3), 514–518.

[36] Furube, A.; Du, L.; Hara, K.; Katoh, R.; Tachiya, M. Ultrafast Plasmon-Induced Electron Transfer from Gold Nanodots into TiO2 Nanoparticles. *J. Am. Chem. Soc.* 2007, *129* (48), 14852–14853.

[37] Seh, ZW; Liu, S.; Low, M.; Zhang, S-Y; Liu, Z.; Mlayah, A.; Han, M-Y Janus Au-TiO2 Photocatalysts with Strong Localization of Plasmonic Near-Fields for Efficient Visible-Light Hydrogen Generation. *Adv. Mater.* 2012, *24* (17), 2310–2314.

[38] Ha, JW; Ruberu, TPA; Han, R.; Dong, B.; Vela, J.; Fang, N. Super-Resolution Mapping of Photogenerated Electron and Hole Separation in Single Metal–Semiconductor Nanocatalysts. *J. Am. Chem. Soc.* 2014, *136* (4), 1398–1408.

[39] Lee, J-S; Shevchenko, EV; Talapin, DV Au–PbS Core–Shell Nanocrystals: Plasmonic Absorption Enhancement and Electrical Doping via Intra-Particle Charge Transfer. *J. Am. Chem. Soc.* 2008, *130* (30), 9673–9675.

[40] Wu, K.; Rodríguez-Córdoba, WE; Yang, Y.; Lian, T. Plasmon-Induced Hot Electron Transfer from the Au Tip to CdS Rod in CdS-Au Nanoheterostructures. *Nano Lett.* 2013, *13* (11), 5255–5263.

[41] Chakrabortty, S.; Yang, JA; Tan, YM; Mishra, N.; Chan, Y. Asymmetric Dumbbells from Selective Deposition of Metals on Seeded Semiconductor Nanorods. *Angew. Chem. Int. Ed.* 2010, *49* (16), 2888–2892.

[42] Habas, SE; Yang, P.; Mokari, T. Selective Growth of Metal and Binary Metal Tips on CdS Nanorods. *J. Am. Chem. Soc.* 2008, *130* (11), 3294–3295.

[43] Mishra, N.; Lian, J.; Chakrabortty, S.; Lin, M.; Chan, Y. Unusual Selectivity of Metal Deposition on Tapered Semiconductor Nanostructures. *Chem. Mater.* 2012, *24* (11), 2040–2046.

[44] Yang, J.; Elim, HI; Zhang, Q.; Lee, JY; Ji, W. Rational Synthesis, Self-Assembly, and Optical Properties of PbS–Au Heterogeneous Nanostructures via Preferential Deposition. *J. Am. Chem. Soc.* 2006, *128* (36), 11921–11926.

[45] Menagen, G.; Mocatta, D.; Salant, A.; Popov, I.; Dorfs, D.; Banin, U. Selective Gold Growth on CdSe Seeded CdS Nanorods. *Chem. Mater.* 2008, *20* (22), 6900–6902.

[46] Carbone, L.; Jakab, A.; Khalavka, Y.; Sönnichsen, C. Light-Controlled One-Sided Growth of Large Plasmonic Gold Domains on Quantum Rods Observed on the Single Particle Level. *Nano Lett.* 2009, *9* (11), 3710–3714.

[47] Saunders, AE; Popov, I.; Banin, U. Synthesis of Hybrid CdS–Au Colloidal Nanostructures†. *J. Phys. Chem. B* 2006, *110* (50), 25421–25429.

[48] Dukovic, G.; Merkle, MG; Nelson, JH; Hughes, SM; Alivisatos, AP Photodeposition of Pt on Colloidal CdS and CdSe/CdS Semiconductor Nanostructures. *Adv. Mater.* 2008, *20* (22), 4306–4311.

[49] Elmalem, E.; Saunders, AE; Costi, R.; Salant, A.; Banin, U. Growth of Photocatalytic CdSe–Pt Nanorods and Nanonets. *Adv. Mater.* 2008, *20* (22), 4312–4317.

[50] Maynadié, J.; Salant, A.; Falqui, A.; Respaud, M.; Shaviv, E.; Banin, U.; Soulantica, K.; Chaudret, B. Cobalt Growth on the Tips of CdSe Nanorods. *Angew. Chem. Int. Ed.* 2009, *48* (10), 1814–1817.

[51] Shemesh, Y.; Macdonald, JE; Menagen, G.; Banin, U. Synthesis and Photocatalytic Properties of a Family of CdS-PdX Hybrid Nanoparticles. *Angew. Chem. Int. Ed.* 2011, *50* (5), 1185–1189.

[52] Alemseghed, MG; Ruberu, TPA; Vela, J. Controlled Fabrication of Colloidal Semiconductor–Metal Hybrid Heterostructures: Site Selective Metal Photo Deposition. *Chem. Mater.* 2011, *23* (15), 3571–3579.

[53] Xia, Y.; Xiong, Y.; Lim, B.; Skrabalak, SE Shape-Controlled Synthesis of Metal Nanocrystals: Simple Chemistry Meets Complex Physics? *Angew. Chem. Int. Ed. Engl.* 2009, *48* (1), 60–103.

[54] Park, K-W; Choi, J-H; Kwon, B-K; Lee, S-A; Sung, Y-E; Ha, H-Y; Hong, S-A; Kim, H.; Wieckowski, A. Chemical and Electronic Effects of Ni in Pt/Ni and Pt/Ru/Ni Alloy Nanoparticles in Methanol Electrooxidation. *J. Phys. Chem. B* 2002, *106* (8), 1869–1877.

[55] Li, X.; Lian, J.; Lin, M.; Chan, Y. Light-Induced Selective Deposition of Metals on Gold-Tipped CdSe-Seeded CdS Nanorods. *J. Am. Chem. Soc.* 2011, *133* (4), 672–675.

[56] Hill, L. J.; Bull, M. M.; Sung, Y.; Simmonds, A. G.; Dirlam, PT; Richey, NE; DeRosa, SE; Shim, I-B; Guin, D.; Costanzo, PJ.; Pinna, N.; Willinger, M-G; Vogel, W.; Char, K.; Pyun, J. Directing the Deposition of Ferromagnetic Cobalt onto Pt-Tipped CdSe@CdS Nanorods: Synthetic and Mechanistic Insights. *ACS Nano.* 2012, *6* (10), 8632–8645.

[57] Sun, Z.; Yang, Z.; Zhou, J.; Yeung, MH; Ni, W.; Wu, H.; Wang, J. A General Approach to the Synthesis of Gold–Metal Sulfide Core–Shell and Heterostructures. *Angew. Chem. Int. Ed.* 2009, *48* (16), 2881–2885.

[58] Shaviv, E.; Schubert, O.; Alves-Santos, M.; Goldoni, G.; Di Felice, R.; Vallée, F.; Del Fatti, N.; Banin, U.; Sönnichsen, C. Absorption Properties of Metal–Semiconductor Hybrid Nanoparticles. *ACS Nano.* 2011, *5* (6), 4712–4719.

[59] Kulakovich, O.; Strekal, N.; Yaroshevich, A.; Maskevich, S.; Gaponenko, S.; Nabiev, I.; Woggon, U.; Artemyev, M. Enhanced Luminescence of CdSe Quantum Dots on Gold Colloids. *Nano. Lett.* 2002, *2* (12), 1449–1452.

[60] Lee, J.; Govorov, AO; Dulka, J.; Kotov, NA Bioconjugates of CdTe Nanowires and Au Nanoparticles: Plasmon–Exciton Interactions, Luminescence Enhancement, and Collective Effects. *Nano. Lett.* 2004, *4* (12), 2323–2330.

[61] Viste, P.; Plain, J.; Jaffiol, R.; Vial, A.; Adam, PM; Royer, P. Enhancement and Quenching Regimes in Metal–Semiconductor Hybrid Optical Nanosources. *ACS Nano.* 2010, *4* (2), 759–764.

[62] Chakrabortty, S.; Xing, G.; Xu, Y.; Ngiam, SW.; Mishra, N.; Sum, TC.; Chan, Y. Engineering Fluorescence in Au-Tipped, CdSe-Seeded CdS Nanoheterostructures. *Small.* 2011, *7* (20), 2847–2852.

[63] Cheng, D.; Xu, Q-H Separation Distance Dependent Fluorescence Enhancement of Fluorescein Isothiocyanate by Silver Nanoparticles. *Chem. Commun.* 2007, No. 3, 248–250.

[64] Pacholski, C.; Kornowski, A.; Weller, H. Site-Specific Photodeposition of Silver on ZnO Nanorods. *Angew. Chem. Int. Ed.* 2004, *43* (36), 4774–4777.

[65] Haldar, KK; Sen, T.; Mandal, S.; Patra, A. Photophysical Properties of Au-CdTe Hybrid Nanostructures of Varying Sizes and Shapes. *Chemphyschem. Eur. J. Chem. Phys. Phys. Chem.* 2012, *13* (17), 3989–3996.

[66] Naiki, H.; Masuhara, A.; Masuo, S.; Onodera, T.; Kasai, H.; Oikawa, H. Highly Controlled Plasmonic Emission Enhancement from Metal–Semiconductor Quantum Dot Complex Nanostructures. *J. Phys. Chem. C* 2013, *117* (6), 2455–2459.

[67] Mongin, D.; Shaviv, E.; Maioli, P.; Crut, A.; Banin, U.; Del Fatti, N.; Vallée, F. Ultrafast Photoinduced Charge Separation in Metal–Semiconductor Nanohybrids. *ACS Nano.* 2012, *6* (8), 7034–7043.

[68] O'Connor, T.; Panov, MS; Mereshchenko, A.; Tarnovsky, AN; Lorek, R.; Perera, D.; Diederich, G.; Lambright, S.; Moroz, P.; Zamkov, M. The Effect of the Charge-Separating Interface on Exciton Dynamics in Photocatalytic Colloidal Heteronanocrystals. *ACS Nano.* 2012, *6* (9), 8156–8165.

[69] Wu, K.; Zhu, H.; Liu, Z.; Rodríguez-Córdoba, W.; Lian, T. Ultrafast Charge Separation and Long-Lived Charge Separated State in Photocatalytic CdS–Pt Nanorod Heterostructures. *J. Am. Chem. Soc.* 2012, *134* (25), 10337–10340.

[70] Mills, A.; Davies, RH; Worsley, D. Water Purification by Semiconductor Photocatalysis. *Chem. Soc. Rev.* 1993, *22* (6), 417–425.

[71] Grätzel, M. Photoelectrochemical Cells. *Nature.* 2001, *414* (6861), 338–344.

[72] Kudo, A.; Miseki, Y. Heterogeneous Photocatalyst Materials for Water Splitting. *Chem. Soc. Rev.* 2008, *38* (1), 253–278.

[73] Kim, SM; Lee, SJ; Kim, SH; Kwon, S.; Yee, KJ; Song, H.; Somorjai, GA; Park, JY Hot Carrier-Driven Catalytic Reactions on Pt–CdSe–Pt Nanodumbbells and Pt/GaN under Light Irradiation. *Nano. Lett.* 2013, *13* (3), 1352–1358.

[74] Amirav, L.; Alivisatos, AP Photocatalytic Hydrogen Production with Tunable Nanorod Heterostructures. *J. Phys. Chem. Lett.* 2010, *1* (7), 1051–1054.